Research Article Vol. 13, No. 5 / 1 May 2023 / Optical Materials Express 1241

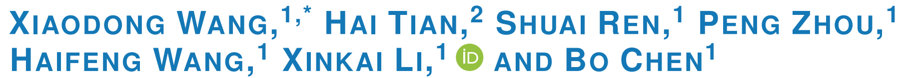

Effects of a simulated high-energy space environment on a LaF_3/MgF_2 multilayer

Xiaodong Wang,[1,*] Hai Tian,[2] Shuai Ren,[1] Peng Zhou,[1] Haifeng Wang,[1] Xinkai Li,[1] and Bo Chen[1]

[1] Changchun Institute of Optics, Fine Mechanics and Physics, Chinese Academy of Sciences, Changchun 130033, China
[2] Science and Technology on Vacuum Technology and Physics Laboratory, Lanzhou 730000, China
[*] wangxiaodong@ciomp.ac.cn

Abstract: Due to their low absorption, the LaF_3/MgF_2 material pair is widely used in the far-ultraviolet space payload. In the space environment, there are plenty of energetic particles (electrons, protons, γ rays, and atomic oxygen) and strong ultraviolet lines. These energetic particles penetrate into the films, and may change the materials' physical and chemical structures. Hence, these energetic particles and ultraviolet lines may degrade the performance of LaF_3/MgF_2. We examined the effect of a simulated high-energy space environment on a LaF_3/MgF_2 multilayer. Dendritic patterns were observed in LaF_3/MgF_2 multilayer irradiated by the 30 keV electrons. The generation mechanism was proposed. This pattern was gradient wrinkle delamination due to the electric discharge, and it was non-uniform, asymmetric. This problem can be avoided by decreasing the substrate heating temperature and lay number (total thickness), and choosing the fluoride material substrate. The LaF_3/MgF_2 multilayer demonstrated no changes after the irradiation of the protons, γ rays, atomic oxygen, and ultraviolet lines.

© 2023 Optica Publishing Group under the terms of the Optica Open Access Publishing Agreement

1. Introduction

Due to high refractive-index-contrast between LaF_3 (high-index material) and MgF_2 (low-index material) and their stability, LaF_3 and MgF_2 was composed a multilayer (ML), which was widely used in far-ultraviolet (FUV). LaF_3/MgF_2 multilayer was used as antireflection and reflection coatings in 193 nm [1] and 157 nm [2] photo-lithography systems because of their lower absorption and larger band gaps, and they achieved higher laser-induced-damage thresholds compared with oxide coatings. A mirror based on LaF_3/MgF_2 ML protected by a dense silicon dioxide protection layer was used in the free-electron laser system at ELETTRA [3]. In astronomical exploration, LaF_3/MgF_2 coatings were used to reflect the emission lines of 121.6 nm (H), 130.4 nm (O), 135.6 nm (O), 140-180 nm (N_2, LBH) [4–12]. Periodic LaF_3/MgF_2 MLs working at 130.4 nm, 135.6 nm, 140-160 nm, 160-180 nm, were used at the ultraviolet imager onboard the Polar satellite [6]. Non-periodic broadband LaF_3/MgF_2 MLs developed by us were also utilized in the wide-field auroral imager onboard Fengyun-3D satellite, and the working wavelength was 140-180 nm [4].

The properties of LaF_3 and MgF_2 were extensively studied [13–21]. Due to the high stress of MgF_2 and large difference in thermal expansion coefficient (CTE) between coatings and the substrate, crakes always appeared [7,22,23]. AlF_3 was used to replace the MgF_2, and a better result was achieved for LaF_3/AlF_3 ML [24]. However, more attention should be paid on the stability of LaF_3/AlF_3 ML in a long time. LaF_3/AlF_3 has not been used in astronomical exploration. Due to its good heritage of the space application, LaF_3/MgF_2 coating is still the first choice for the optical payloads.

In the space, there are plenty of energetic particles (protons, electrons, γ rays, and atomic oxygen (AO)) and ultraviolet (UV) lines. When optical MLs are exposed to these energetic particles, their optical performances may degrade over time. It was found that the surface roughness, optical loss, stress of LaF_3 thin films were improved after thermal annealing and UV light irradiation

#484603 https://doi.org/10.1364/OME.484603
Journal © 2023 Received 4 Jan 2023; revised 26 Feb 2023; accepted 24 Mar 2023; published 10 Apr 2023

Optical Materials EXPRESS

at 193 nm [25]. It was found that there were no major radiation-induced changes in reflectance for LaF_3/MgF_2 mirror after 250 krad of γ ray radiation from a ^{60}Co gamma source [26]. The influence of protons and electrons irradiation on MgF_2 substrate was extensively investigated in FUV [27,28]. However, there are no reports about the influence of protons, electrons, and AO irradiation on LaF_3/MgF_2 ML. Here, the effects of a simulated high-energy space environment on the LaF_3/MgF_2 ML were investigated. In 2022, the Lyman-alpha Solar Telescope (LST) onboard the Advanced Space-based Solar Observatory (ASO-S) Satellite has been launched at this space environment (an altitude of 720 km) [29,30]. Our fabricated LaF_3/MgF_2 ML was used in the LST.

2. Design, fabrication, irradiation experiment, and characterization

LaF_3/MgF_2 was designed by Optilayer software (version 10.48 h) [31], quarterwave (QW) ML design was used, the working wavelength was 121.6 nm, and the incident angle was 17 degree. The nominal thicknesses of LaF_3 and MgF_2 were 14.6 nm and 19.7 nm, respectively.

The purity of LaF_3 and MgF_2 was 99.95%, and 99.99%, respectively. MgF_2 and LaF_3 were deposited by the thermal evaporation method. They were fabricated by a molybdenum boat with a rate of 0.2 nm/s. The base pressure of chamber was pumped by molecular pump to be 3.0×10^{-4} Pa. The thickness was controlled by the quartz crystal.

We carried out the experiment of a simulated high-energy space environment in Lanzhou Institute of Physics (China). Electron gun (EFHS-100-2W, STAIB INSTRUMENTE Company, Germany) was used to produce the electrons. Dual-beam proton accelerator (2.0MVSINGLETRONDUAL, High Voltage Engineering Company) was used to produce the protons. Coaxial AO simulation facility developed by Lanzhou Institute of Physics was used to produce AO. ^{60}Co Source was used to produce γ rays for the total ionizing dose (TID) irradiation experiment. The Mercury-xenon lamp with a power of 500 W was used to produce the UV lines. The test flux and total dose were given in Table 1.

Table 1. A simulated high-energy space environment and experimental information.

Irradiation	Energy	Test Flux	Total Dose	Test Time (Hours)
Proton	100 keV	1.6×10^{10} cm^{-2} s^{-1}	3.54×10^{13} cm^{-2}	2
Electron	30 keV	4.8×10^{9} cm^{-2} s^{-1}	5.67×10^{14} cm^{-2}	32
AO	5 eV	1.0×10^{20} m^{-2} s^{-1}	2.76×10^{24} m^{-2}	7
TID	—	50 rad [Si]	4.44×10^{7} rad [Si]	248
UV	—	3.162×10^{3} W/m^2	1.94×10^{10} J/m^2	1704

The reflectance in the FUV region was measured by our own developed reflectometer with a deuterium lamp, and the details about this system can be found in Ref. [32]. The film surfaces were observed by the laser interferometer (ZYGO, GPI/XP).

3. Results and discussion

Figure 1 shows reflectance curves of samples after protons, TID, AO, and UV irradiations, and synergetic effect of four kinds of irradiations for the sample is also given. It was found that there were no significant changes of reflectance at 121.6 nm after theses irradiations. These samples with 9 layers were deposited on a fused silica substrate with a heating temperature of 320 degree.

As shown in Fig. 2, it was well known that LaF_3/MgF_2 ML was prone to crack [7,22,23]. There are two reasons for this phenomenon: one was large difference of the CTE between fluoride films and fused silica substrate, the other was high intrinsic stress of fluoride films, especially MgF_2.

Different from this common phenomenon, we found that there were dendritic patterns in LaF_3/MgF_2 coatings after 30 keV electron irradiation. Dendritic patterns can be observed by

Optical Materials EXPRESS

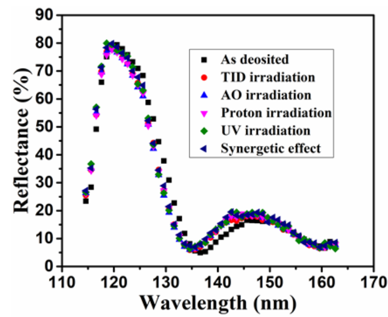

Fig. 1. Reflectance curves of samples after protons, TID, AO, and UV irradiations.

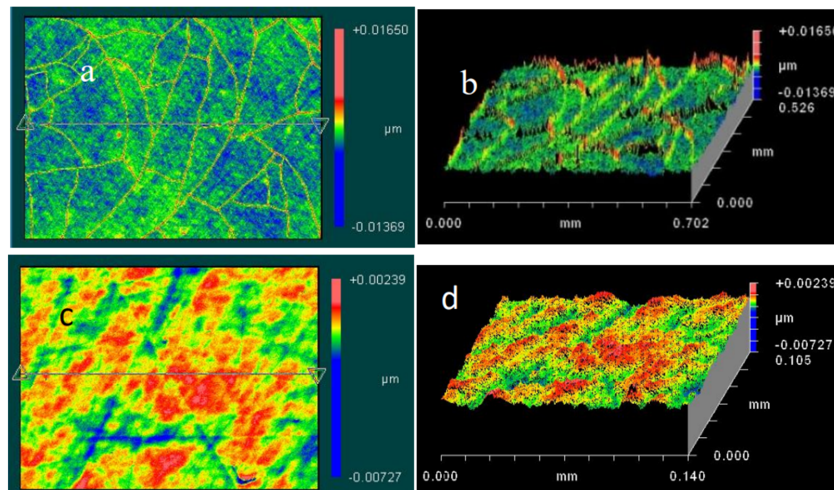

Fig. 2. Cracks in LaF_3/MgF_2 coating: (a) the plane view, and (b) the oblique view. For comparison, the pictures (c, d) for samples without cracks are also given.

naked eyes in a specific angle and a laser interferometer, and it was dependent on the thickness of fluoride films, the substrate heating temperature, and the substrate materials.

As shown in Fig. 3, with increasing of the layer number from 6 to 10 (a-c) and the temperature from 220 to 240 degree (d-e), dendritic patterns became more obvious. As shown in Fig. 3(f)–3 g, we replaced the fused silica substrate by the MgF_2 substrate, the dendritic patterns disappeared.

To better understand the dendritic patterns, we gave different views in Fig. 4(b)–4(e). The dendritic patterns were located at the edge of the coatings. They were wrinkle delamination. The magnitude of the wrinkles decreased from the edge to the center of the coating. For comparison, surface map of bare substrate was also given. Surface map of coatings before 30 keV electron irradiation was same to Fig. 4(a), for brevity, this picture was not provided. In addition, as shown in Fig. 4(f), dendritic patterns destroyed the reflectance of the coating. The reflectance reduced from 74.3% to 43.7%, and the central wavelength shifted to the longer wavelength by 6 nm.

To understand the generation mechanism of the dendritic patterns, Casino v2.4.8.1 software [33] was used to simulate the electron irradiation on LaF_3/MgF_2 coatings. Figure 5 shows 30 keV electron beam trajectories in (a) the mirror and (b) the coatings. It can be seen that most of the electrons transmitted the coatings and dispersed in the substrate, and the dispersion distance was within 10 μm. As shown in Fig. 5(c), a large number of the electrons accumulated in a narrow insulative area, they induced a huge electric field intensity of 2.56×10^{10} V/m. Thus,

Optical Materials EXPRESS

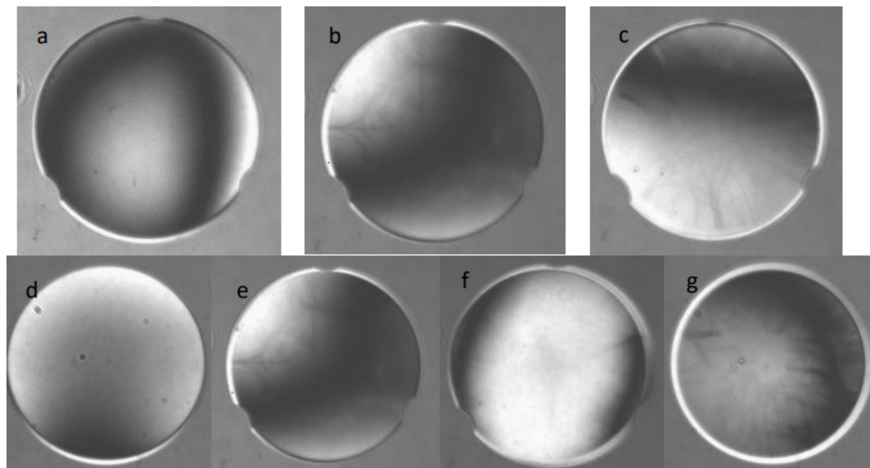

Fig. 3. (a-c) Dendritic patterns in LaF_3/MgF_2 coatings with different periodic numbers after 30 keV electron irradiation: (a) 6 layers, (b) 8 layers, (c) 10 layers. The substrate temperature was 240 degree, and the substrate was fused silica. (d-e) Dendritic patterns in LaF_3/MgF_2 coatings with different substrate temperature after 30 keV electron irradiation: (d) 220 degree, (e) 240 degree. The layer number was 8, and the substrate was fused silica. (f-g) Dendritic patterns in LaF_3/MgF_2 coatings with different substrate materials after 30 keV electron irradiation: (f) MgF_2 substrate, (g) fused silica substrate. The layer number was 7, and the substrate temperature was 290 degree.

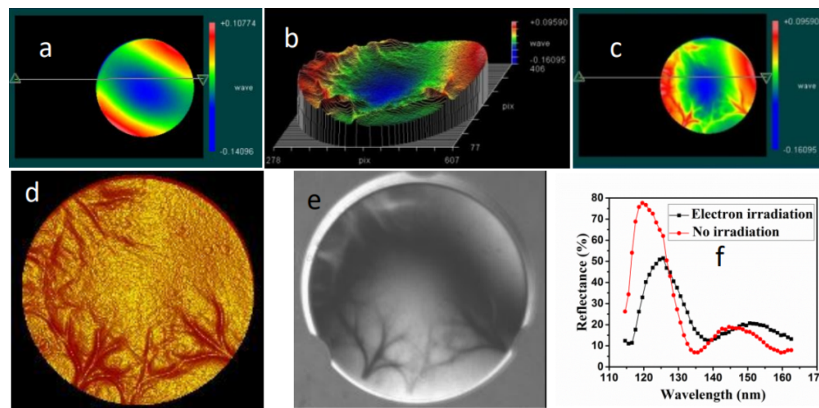

Fig. 4. (a) Surface map of bare substrate. Different views of the dendritic patterns in LaF_3/MgF_2 coatings on the fused silica substrate: (b) oblique plot, (c) surface map, (d) solid map, (e) intensity map. The layer number was 9, and the substrate temperature was 340 degree. (f) The reflectance variance of LaF_3/MgF_2 on the fused silica substrate after the electron irradiation. The layer number was 9, the substrate temperature was 340 degree, and the incident angle was 17 degree.

they generated the electric discharge nearby the conductive metal edge (supporting sample), and they released the huge thermal energy. Significant temperature increase resulted in thermal stress enhancement, which leaded to the appearance of the dendritic patterns at the edge of the coatings. As shown in Eq. (1), the total stress includes thermal stress, intrinsic stress and extrinsic stress due to external load. It was well known, high substrate temperature (200-300 °C) during the deposition resulted in a lower intrinsic stress and a higher thermal stress for the MgF_2 film [17]. Thus, our fabricated LaF_3/MgF_2 ML has a strong thermal stress. The extrinsic stress due to the electron irradiation was essentially a thermal stress, which can be calculated by Eq. (2), where E is the Young modulus, ν is the Poisson ratio of the coating, α_{sub} and α_{film} are the TECs of the substrate and film, respectively, T is the room temperature, and T_e is the heating temperature due to the electric discharge of the electron irradiation.

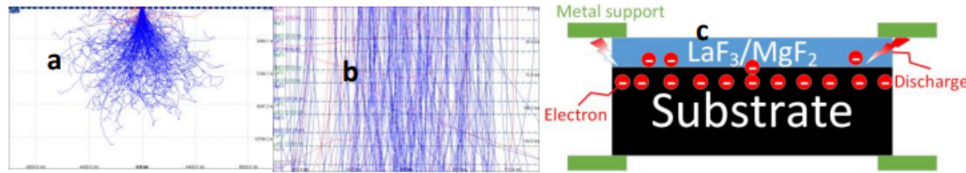

Fig. 5. Simulation results of 30 keV electron beam trajectories in (a) the mirror and (b) the LaF_3/MgF_2 coatings by Casino v2.4.8.1 software. The electron beam beats from the coatings to the substrate of the mirror, the blue lines denote the forward electrons and the red lines denote the reverse. The number of used electrons is 7.12152×10^5. Beam area has a radius of 200 nm. The density is 5.67×10^{14} e/cm^2 (as shown in Table 1).

Traditionally, as shown in Fig. 6, the film stress brings about a curvature change on the substrate. The tensile stress makes the substrate surface become concave, and the large tensile stress generates the cracks. The compressive stress makes the substrate surface become convex, and the large compressive stress generates the buckling delamination of the coating. The traditional stress can be calculated by Eq. (3), where d_s and d_f are the thicknesses of the substrate and the film, respectively, R_e and R_0 are substrate radii before (R_0) and after (R_e) electron irradiation. Surface figure variance and the delamination due to the traditional stress are uniform and isotropic [34]. On contrary, here, as shown in Fig. 4(b), the stress was mainly located at the periphery of the coating, and it was asymmetric, anisotropic, and not uniform. The stress decreased from the edge to the center of the coating. As shown in Fig. 4(b) and 4(c), although there were wrinkles at the edge of the coating, the coating had no changes in the PV value, and there was no dendritic pattern at the center of the coating. In other words, this asymmetric tensile stress generated a different variance in the surface figure, it cannot be characterized by a curvature change on the substrate, and it thus cannot be calculated by the Eq. (3). Figure 7 illustrates the formation of the wrinkle delamination due to the asymmetric tensile stress. There was the largest stress at the outmost of the coating, where the adhesion may be weak due to some defects. This stress was large enough to overcome the adhesion between the film and the substrate, and the film wrinkled and delaminated. The gradient stress caused the gradient wrinkles from the edge to the center of the coating. The non-uniformity of the thermal tensile stress was the formation reason for this wrinkle delmaination.

$$\sigma_{total} = \sigma_{therm} + \sigma_{intr} + \sigma_{ext} \tag{1}$$

$$\sigma_{ext} = \left(\frac{E}{1-\vartheta}\right)_{film} (\alpha_{sub} - \alpha_{film})(T - T_e) \tag{2}$$

$$\sigma_{total} = \frac{E}{1-\vartheta}\frac{d_s^2}{6d_f}\left(\frac{1}{R_e} - \frac{1}{R_0}\right) \tag{3}$$

Optical Materials EXPRESS

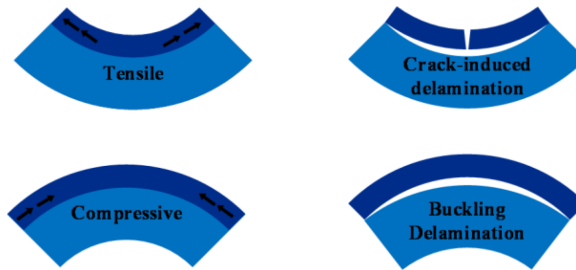

Fig. 6. Illustration of the effect of a tensile or compressive deposited thin film on the substrate bending [34].

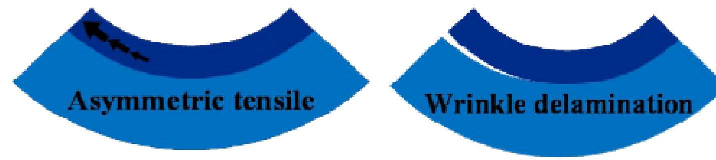

Fig. 7. Illustration of asymmetric-tensile-stress-induced wrinkle delamination.

To avoid this wrinkle delamniantion, the total stress of LaF_3/MgF_2 must be reduced. In other words, as shown in Eq. (1), the intrinsic and thermal stress must be reduced. Finally, we made a tradeoff between the reflectance and dendritic patterns. We reduced the substrate heating temperature and the thickness of coatings to avoid the dendritic patterns after the electron irradiation and the cracks in LaF_3/MgF_2. As shown in Fig. 8, with decreasing of layers, reflectance of sample decreased from 74.7% to 68.1%, and the substrate heating temperature was 220 degree; with decreasing of substrate heating temperature, reflectance of sample decreased from 75.6% to 68.1%, and the layer number of samples was 6. Variance of dendritic patterns dependence on the substrate heating temperature and the thickness of coatings can be found in Fig. 3. Finally, LaF_3/MgF_2 with a layer number of 6 on the fused silica was chosen, and the substrate heating temperature was 220 degree. No dendritic pattern was observed, and surface morphology was same to Fig. 3(a) and 3(d). As shown in Fig. 8, the measured reflectance was 68.1% at 121.6 nm, and the incident angle was 17 degree.

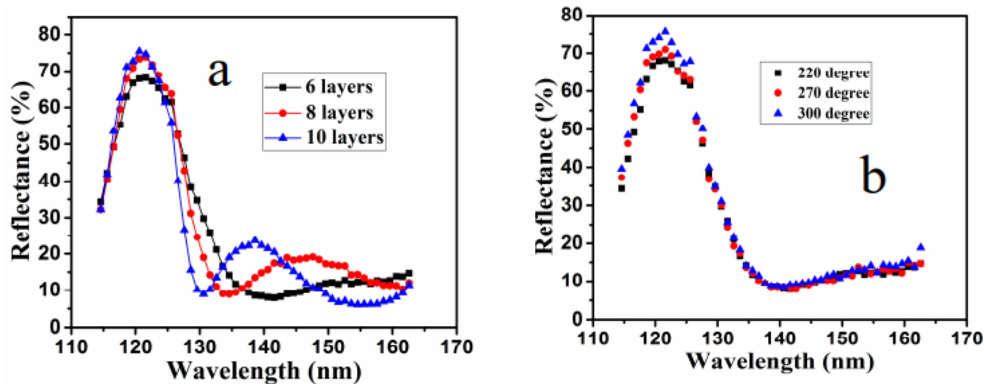

Fig. 8. Experimental reflectance curves of LaF_3/MgF_2 ML with different layers (a) and substrate heating temperature (b).

Optical Materials EXPRESS

4. Conclusions

The QW 121.6 nm LaF_3/MgF_2 ML was fabricated. We carried out a simulated space environment test on the MLs. No significant changes were found after the proton, γ ray, AO, and UV irradiations. Unexpectedly, dendritic patterns were found by naked eyes and the reflectance degraded for the coatings after 30 keV electron irradiation, and these patterns were gradient wrinkle delaminations characterized by the laser interferometer. The magnitude of the wrinkles gradually decreased from the edge to the center of the coating. The wrinkles were non-uniform, asymmetric. The large temperature enhancement caused by the electric discharge was the formation mechanism of the wrinkle mechanism. By decreasing the layer number and the substrate heating temperature, that is, by reducing the intrinsic and thermal stress, a LaF_3/MgF_2 ML without the wrinkles and cracks was obtained, and it has a reflectance of 68.1% at 121.6 nm.

Our job provided a thorough investigation on the space environment adaptability for LaF_3/MgF_2 MLs, and the synergetic effect of proton, γ ray, AO, and UV irradiations was also given.

Funding. National Natural Science Foundation of China (12273040); Joint Fund of Astronomy (U2031122).

Acknowledgments. We thank Professor Alexander Tikhonravov from Moscow State University for fruitful discussions of characterization of optical constant of MgF_2 films.

Disclosures. The authors declare no conflicts of interest.

Data Availability. Data underlying the results presented in this paper are not publicly available at this time but may be obtained from the authors upon reasonable request.

References

1. C. Liu, M. Kong, and B. Li, "Performance optimization of 193 nm antireflective coatings with wide incident angle ranges on strongly curved spherical substrates," Opt. Express **26**(15), 19524–19533 (2018).
2. S. Niisaka, T. Saito, J. Saito, A. Tanaka, A. Matsumoto, M. Otani, R. Biro, C. Ouchi, M. Hasegawa, Y. Suzuki, and Kazuho Sone, "Development of optical coatings for 157-nm lithography. I. Coating materials," Appl. Opt. **41**(16), 3242–3247 (2002).
3. S. Günster, D. Ristau, A. Gatto, N. Kaiser, M. Trovó, and M. Danailov, "Storage ring free-electron lasing at 176 nm—dielectric mirror development for vacuum ultraviolet free-electron lasers," Appl. Opt. **45**(23), 5866–5870 (2006).
4. X. Zhang, B. Chen, and F. He, *et al.*, "Wide-field auroral imager onboard the Fengyun satellite," Light: Sci. Appl. **8**(1), 47 (2019).
5. S. B. Mende, H. Heetderks, H. U. Frey, M. Lampton, S. P. Geller, R. Abiad, O. H. W. Siegmund, A. S. Tremsin, J. Spann, H. Dougani, S. A. Fuselier, A. L. Magoncelli, M. B. Bumala, S. Murphree, and T. Trondsen, "Far ultraviolet imaging from the image spacecraft. 2. Wideband FUV imaging," Space Sci. Rev. **91**(1/2), 271–285 (2000).
6. M. R. Torr, D. G. Torr, M. Zukic, R. B. Johnson, J. Ajello, P. Banks, K. Clark, K. Cole, C. Keffer, G. Parks, B. Tsuratani, and J. Spann, "A far ultraviolet imager for the International Solar-Terrestrial Physics Mission," Space Sci. Rev. **71**(1-4), 329–383 (1995).
7. X. Wang, B. Chen, and L. Yao, "Design and fabrication of far-ultraviolet reflective broadband filter based on dielectric materials," Appl. Spectrosc. **72**(6), 943–946 (2018).
8. N. Gutiérrez-Luna, P. López-Reyes, C. Honrado-Benítez, L. Espinosa-Yáñez, A. RíosFernández, L. V. Rodríguez-de Marcos, M.A. Quijada, and J. I. Larruque, "Mirrors for improved FUV space observations," Proc. SPIE **11444**, 1144478 (2020).
9. J. I. Larruquert, A. Marco Malvezzi, L. Marcos, A. Rodríguez-de Giglia, N. Gutiérrez-Luna, L. Espinosa-Yáñez, C. Honrado-Benítez, J. A. Aznárez, G. Massone, G. Capobianco, S. Fineschi, and S. Nannarone, "Polarizers tuned at key far-UV spectral lines for space instrumentation," Proc. SPIE **10235**, 102350 K (2017).
10. X. Wang, B. Chen, T. Huo, and H. Zhou, "Design of first-order 121.6 nm minus filters," Appl. Spectrosc. **72**(10), 1498–1502 (2018).
11. X. Wang, B. Chen, T. Huo, and H. Zhou, "Design of second-order 121.6-nm narrowband minus filters using asymmetrically apodized thickness modulation," Appl. Phys. B **124**(7), 139 (2018).
12. X. Wang and B. Chen, "Design of dual-band cold mirrors," Sci. Rep. **7**(1), 15402 (2017).
13. M. Zukic, D. G. Torr, J. F. Spann, and M. R. Torr, "Vacuum ultraviolet thin films 2: Vacuum ultraviolet all-dielectric narrowband filters," Appl. Opt. **29**(28), 4293–4302 (1990).
14. G. Liu, Q. Xiao, Y. Jin, W. Zhang, H. He, and Z. Fan, "Mechanical stress in 355 nm LaF_3/MgF_2 high reflectors with various layer-pair number and methods for reduction," Vacuum **84**(6), 778–781 (2010).
15. L. Rodríguez-de Marcos, J. I. Larruquert, J. A. Méndez, and J. A. Aznárez, "Multilayers and optical constants of various fluorides in the far UV," Proc. SPIE **9627**, 96270B (2015).

Optical Materials EXPRESS

16. J. Ullmann, H.-G. Keck, R. Thielsch, H. Uhlig, and N. Kaiser, "Mechanical stress in fluoride coatings," Proc. SPIE **3738**, 136–147 (1999).
17. R. Thielsch, J. Heber, H. Uhlig, and N. Kaiser, "Development of mechanical stress in fluoride multilayers for UV applications," Proc. SPIE **5250**, 127–136 (2004).
18. D. Ristau, S. Günster, S. Bosch, A. Duparré, E. Masetti, J. Ferré-Borrull, G. Kiriakidis, F. Peiró, E. Quesnel, and A. Tikhonravov, "Ultraviolet optical and microstructural properties of MgF_2 and LaF_3 coatings deposited by ion-beam sputtering and boat and electron-beam evaporation," Appl. Opt. **41**(16), 3196–3204 (2002).
19. S. Schröder, H. Uhlig, A. Duparré, N. Kaiser, F. Angewandte, and D. Jena, "Nanostructure and optical properties of fluoride films for high-quality DUV/VUV optical components," Proc. SPIE **5963**, 59630R (2005).
20. D. R. J. Kolbe, H. Kelsser, T. Hofmann, F. Meyer, and H. Schink, "Optical properties and damage thresholds of dielectric UV/VUV-coatings deposited by conventional evaporation, IAD and IBS," Proc. SPIE **1624**, 221–235 (1992).
21. L. Dumas, E. Quesnel, J.-Y. Robic, and Y. Pauleau, "Characterization of magnesium fluoride thin films deposited by direct electron beam evaporation," J. Vac. Sci. Technol., A **18**(2), 465–469 (2000).
22. P. López-Reyes, B. Perea-Abarca, C. Honrado-Benítez, N. Gutiérrez-Luna, A. Ríos-Fernández, L. V. Rodríguez-de Marcos, and J. I. Larruquert, "Optimization of the deposition parameters of MgF_2/LaF_3 narrowband reflective FUV multilayers," Opt. Mater. Express **11**(6), 1678–1691 (2021).
23. M. Granata, A. Amato, M. Bischi, M. Bazzan, G. Cagnoli, M. Canepa, M. Chicoine, A. Di Michele, G. Favaro, D. Forest, and G. M. Guidi, "Optical and mechanical properties of Ion-Beam-Sputtered MgF_2 thin films for Gravitational Wave Interferometers," Phys. Rev. Appl. **17**(3), 034058 (2022).
24. P. López-Reyes, C. Honrado-Benítez, N. Gutiérrez-Luna, A. Ríos-Fernández, L. V. Rodríguez-de Marcos, and J. I. Larruquert, "Far-UV reflectance and stress of narrowband AlF_3/LaF_3 multilayers," Opt. Mater. Express **12**(2), 489–502 (2022).
25. C. Lee, M. Liu, M. Kaneko, K. Nakahira, and Y. Takano, "Influence of thermal annealing and ultraviolet light irradiation on LaF3 thin films at 193 nm," Appl. Opt. **44**(32), 6921–6926 (2005).
26. C. E. Keffer, M. R. Torr, M. Zukic, J. F. Spann, D. G. Torr, and J. Kim, "Radiation damage effects in far-ultraviolet filters, thin films, and substrates," Appl. Opt. **33**(25), 6041–6045 (1994).
27. D. F. Heath and P. A. Sacher, "Effects of a simulated high-energy space environment on the ultraviolet transmittance of optical materials between 1050 A and 3000 A," Appl. Opt. **5**(6), 937–943 (1966).
28. G. Hass and W. R. Hunter, "Laboratory experiments to study surface contamination and degradation of optical coatings and materials in simulated space environments," Appl. Opt. **9**(9), 2101–2110 (1970).
29. B. Chen, H. Li, and K. Song, *et al.*, "The Lyman-alpha Solar Telescope (LST) for the ASO-S mission-II. design of LST," Res. Astron. Astrophys. **19**(11), 159 (2019).
30. H. Li, B. Chen, and L. Feng, *et al.*, "The Lyman-alpha Solar Telescope (LST) for the ASO-S mission-I. Scientific objectives and overview," Res. Astron. Astrophys. **19**(11), 158 (2019).
31. A. V. Tikhonravov and M. K. Trubetskov, OptiLayer thin film software, http://www.optilayer.com.
32. H. Wang, X. Wang, B. Chen, Y. Wang, and S. Mao, "EUV multilayer mirrors in solar X-EUV Imager," Optik **204**, 164213 (2020).
33. D. Drouin, A. R. Couture, D. Joly, X. Tastet, V. Aimez, and R. Gauvin, "CASINO V2.42-A fast and easy-to-use modeling tool for scanning electron microscopy and microanalysis users," Scanning **29**(3), 92–101 (2007).
34. S. Massahi, L. M. Vu, D. D. M. Ferreira, F. E. Christensen, N. Gellert, P. L. Henriksen, S. Svendsen, A. S. Jegers, M. Collon, B. Landgraf, D. Girou, A. Thete, B. Shortt, I. Ferreira, and M. Bavdaz, "Balancing of residual stress in thin film iridium by utilizing chromium as an underlayer," Proc. SPIE **11444**, 114444N (2020).

159.226.100.203 {ts 2024-04-22 04:41:04}